Neutron Reflectivity Measurements for the Interfacial Characterization of Polymer Thin Film Photoresists

Eric K. Lin[a], Christopher L. Soles[a], Wen-li Wu[a], Sushil K. Satija[b]
Qinghuang Lin[c], Marie Angelopoulos[c]

[a] Polymers Division and [b]Center for Neutron Research, National Institute of Standards and Technology, Gaithersburg, MD 20899

[c] IBM T. J. Watson Research Center, Yorktown Heights, NY 10598

ABSTRACT

As photoresist layers become thinner with shorter imaging wavelengths, interfacial structure and transport issues are increasingly important to photoresist performance. High spatial resolution interfacial measurement methods are needed both to observe processes over length scales (< 20 nm) relevant to lithographic structures and to understand fundamental transport issues that determine the ultimate feature resolution. In this work, neutron reflectivity measurements are used to provide high spatial resolution measurements of the interfacial behavior in model polymer photoresist materials. Bilayer samples are prepared with a lower layer of poly(hydroxystyrene) (PHS) with or without a photoacid generator, bis(p-tert-butylphenyl) iodonium perfluorooctanesulfonate (PFOS), and an upper layer of either hydrogenated or deuterated poly(methyl methacrylate) (PMMA). We measure the initial rates of diffusion by measuring the depth profiles of the bilayer structure as a function of post-apply baking conditions, post-exposure bake temperature, (above and below the glass transition temperature of the polymers) and time.

Keywords: Neutron reflectivity, interfacial broadening, polymer interdiffusion

INTRODUCTION

The continuing drive to fabricate smaller feature sizes in integrated circuits includes the development of photoresist materials optimized for wavelengths of 193 nm and shorter. Future photoresist imaging layers for the fabrication of integrated circuits must become thinner because of the large absorption of shorter wavelength radiation by current polymeric materials. Several solutions have been proposed including the incorporation of etch resistance to the photoresist polymer or the adoption of a bilayer structure where a thin imaging layer is placed on top of an underlayer. Additionally, the allowable resolution of the lithographic process, line-edge or sidewall roughness, must also decrease to less than (10 – 20) nm. Over these small length scales, the transport of small molecule additives and the interfacial development between exposed and unexposed areas may dominate lithographic performance. High spatial resolution measurements and fundamental understanding of interfacial structure and transport issues are needed to help develop future photoresist materials.

The prevailing lithographic technology utilizes chemically amplified photoresists through acid catalysis. Basic transport and interfacial structure issues such as photoacid generation, acid diffusion, deprotection reaction kinetics, and possible phase segregation between the protected and deprotected polymer need to be understood to optimize process parameters. For example, acid diffusion during the post-exposure bake (PEB) has a marked effect on the final feature structure [1]. If acid diffusion proceeds into the unexposed part of the resist film, then the image degrades and there is a loss of resolution. Many experimental methods have been developed to measure and quantify acid diffusion in photoresist matrices including inferring diffusion from the developed image, pH sensitive dye fluorescence measurements [2], IR spectroscopy [3], Rutherford Backscattering Spectrometry (RBS) [4], and Secondary Ion Mass Spectrometry (SIMS) [5]. These measurements have provided important insight into acid diffusion rates, but did not have sufficient resolution to observe acid diffusion or reactions over length scales commensurate with the line-edge roughness (< 40 nm). It has also been

noted that diffusion coefficients determined using these longer length scale measurements could not account for observed spreads in the line widths (assuming Fickian diffusion) [6].

Polymer interdiffusion and polymer/polymer interface issues may also play an important role in the ultimate resolution of the lithographic process. For example, phase separation between the protected and deprotected polymer in transition regions between the exposed and unexposed areas of a photoresist has been identified as a contributor to line-edge roughness [7]. The kinetics of interface formation and/or interdiffusion over short distances may play an important role in the ultimate resolution of a lithographic process. There are many variables that strongly affect the rate at which incompatible or partially compatible polymer pairs (protected and deprotected polymers) such as the thermodynamic interaction energy, the glass transition temperatures of the polymers, the relative molecular mass of the polymers, and the polymer composition (for copolymers). In addition to processes such as acid diffusion and dissolution, it is important to understand the thermodynamics and kinetics of polymeric interfacial regions to optimize photoresist formulations.

In this work, we explore the use of neutron reflectometry to measure and characterize the interfacial structure between two model photoresist polymer layers with high spatial resolution. Neutron reflectometry has been previously used to study the interdiffusion of miscible polymers over distances less than 20 nm [8-11] and to measure the interfacial width of immiscible polymer layers [12]. With sufficient contrast to neutrons, film thicknesses, interfacial profiles, and interfacial widths may be determined with 0.1 nm resolution. We prepare bilayer samples on silicon substrates with a lower layer of poly(hydroxystyrene) (PHS) with and without a photoacid generator (PAG) and an upper layer of deuterated or hydrogenated poly(methyl methacrylate) (PMMA). We compare the interfacial profile of bilayer samples prepared with PHS/PAG layers that were post-apply baked (PAB) for short times (3 min) and very long times (20 h). We also measure interdiffusion between the PHS/PAG and the PMMA layers at temperatures below the glass transition temperature, Tg, of both polymers, above the Tg of one polymer and below the Tg of the other polymer, and above the Tg's of both polymers. We find that extensive PAB times results in denser PHS/PAG films than the short PAB. We also find that the polymer layers do not interdiffuse until the baking temperature is above the Tg's of both polymers. Longer time experiments with only the polymer materials suggest that PHS and PMMA are partially miscible and exhibit an unusual initial broadening and then sharpening of the interfacial width.

EXPERIMENT

Bilayer samples were prepared on <111> single crystal silicon wafers, 5 mm thick and 75 mm in diameter. Before depositing the polymer thin films, the silicon substrates were extensively cleaned in oxygen plasma to remove organic contaminants. The substrates were then immersed in a buffered hydrofluoric acid etch solution to remove the native oxide layer. After rinsing with ultrapure water (resistivity > 18 MΩ·cm), the silicon substrates were placed into a UV/ozone cleaner to reproducibly prepare the native oxide layer. The lower polymer layers of poly(hydroxystyrene) (PHS) were spin-coated from solutions of propylene glycol methyl ether acetate (PGMEA) with mass fractions of either 2 % or 5 %. The molecular weight of the PHS polymer is 3070 g/mol [13] with a polydispersity index of 1.23. The glass transition temperature, Tg, of PHS is approximately 150 °C. In most samples, a photoacid generator, bis(p-tert-butylphenyl) iodonium perfluorooctanesulfonate (PFOS), was added with the PHS with a solids mass fraction of 5 %. The PHS/PFOS layers were then either annealed for 3 min at 140 °C (short anneal) or for at least 12 h at 120 °C (long anneal). The upper polymer layers consisted of either deuterated or hydrogenated poly(methyl methacrylate) (d-PMMA or h-PMMA). The molecular weight of the d-PMMA was 135000 g/mol and that of the h-PMMA was 125000 g/mol with polydispersity indices less than 1.15. The Tg's of both PMMA polymers are 115 °C. The PMMA polymers were spin-coated from o-xylene solutions with mass fractions of 2.5 % or 3.0 % onto cleaned glass slides. The PMMA layers were then floated onto ultrapure water and transferred onto the lower PHS layers. The bilayer samples were then dried under high vacuum at 25 °C for at least 12 h. Samples containing PFOS were exposed to UV radiation from a lamp with a nominal wavelength of 265 nm. The dose on the samples was approximately 75 mJ/cm^2. Neutron reflectivity measurements were performed on the same sample after various annealing conditions. The samples were annealed in a slotted aluminum block under vacuum at temperatures ranging from 80 °C to 160 °C. After annealing, the samples were rapidly cooled to room temperature on a cool aluminum block (< 30 s) to halt diffusion.

Neutron reflectivity measurements were performed on the NG7 Reflectometer at the National Institute of Standards and Technology Center for Neutron Research. The wavelength, λ, of the incident neutrons was 4.75 Å with a wavelength spread, $\Delta\lambda/\lambda = 0.2$. The neutron beam was sent at grazing incident angles, θ_i, to the sample surface and detected at the specular condition where the detection angle, θ_r, is equal to θ_i. The data are plotted as the logarithm of the reflectivity (the

ratio of the reflected intensity to the incident intensity) versus q where $q = \frac{4\pi}{\lambda}\sin\theta$ and is the momentum transfer of the neutron normal to the sample surface. The reflectivity data are taken under ambient atmospheric conditions. The neutron reflectivity data are modeled using nonlinear least-squares fits with a recursive multilayer method [14]. In this procedure, model real space depth profiles of the neutron scattering length density are generated. Then, the reflectivity is calculated and compared with the experimental data. Model parameters such as the polymer layer thickness or interfacial width are varied to minimize the difference between the model calculation and the reflectivity data. All data in the paper and in the figures are presented with the standard uncertainty of the measurement.

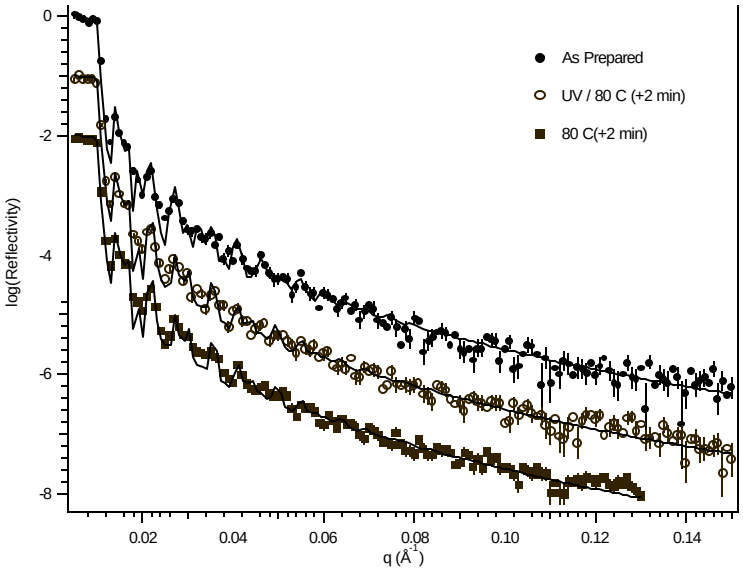

Figure 1a. The symbols are the neutron reflectivity data for a bilayer sample with a lower layer of PHS/PFOS and an upper layer of h-PMMA after various thermal treatments. The data are vertically offset for clarity and are presented with error bars representing the standard uncertainty of the measurement. The solid lines represent the best fit to the experimental data.

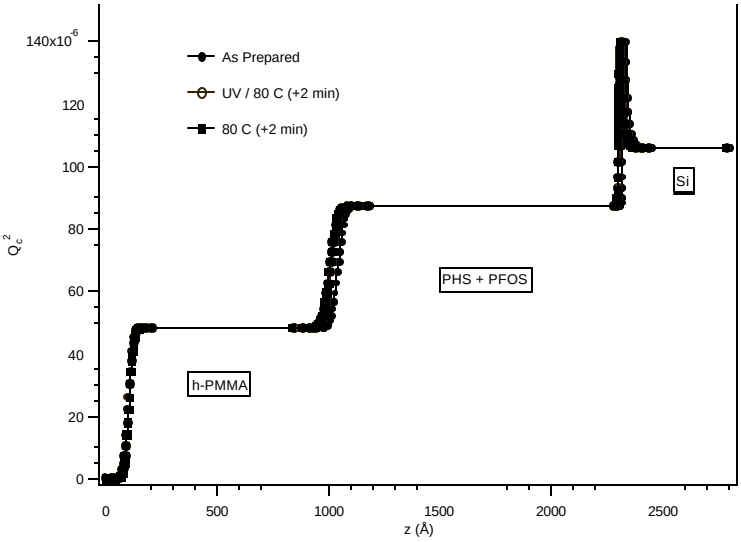

Figure 1b. Real space depth profiles representing the best model fits to the neutron reflectivity data in Figure 1a of a bilayer sample with a lower layer of PHS/PFOS and an upper layer of h-PMMA.

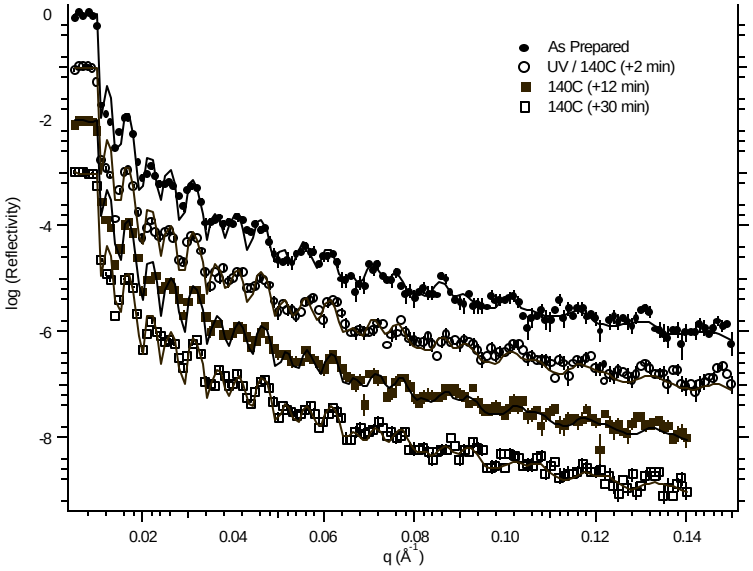

Figure 2a. The symbols are the neutron reflectivity data for a bilayer sample with a lower layer of PHS/PFOS and an upper layer of h-PMMA after various thermal treatments. The data are vertically offset for clarity and are presented with error bars representing the standard uncertainty of the measurement. The solid lines represent the best fit to the experimental data.

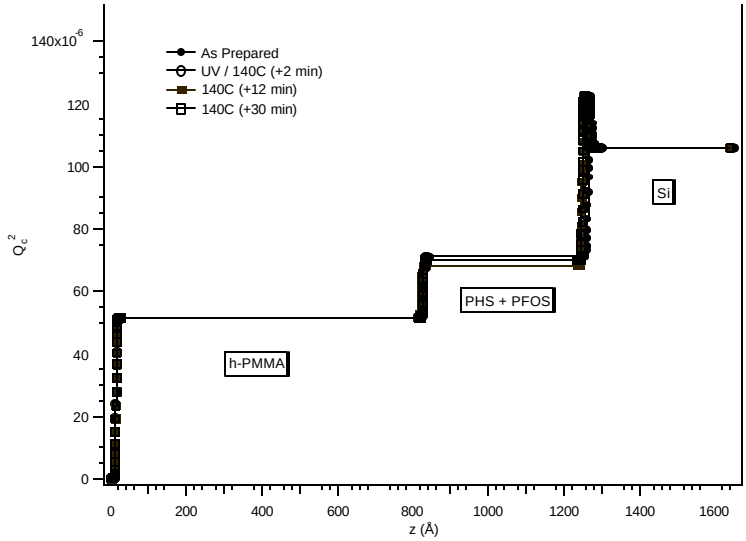

Figure 2b. Real space depth profiles representing the best model fits to the neutron reflectivity data in Figure 2a of a bilayer sample with a lower layer of PHS/PFOS and an upper layer of h-PMMA after various processing steps.

RESULTS AND DISCUSSION

Figure 1a shows a typical set of neutron reflectivity data as well as the best model fits to the data from a bilayer sample consisting of a lower layer of PHS/PFOS (1268 ± 1) Å thick and an upper layer of h-PMMA, (811 ± 1) Å thick. The PHS/PFOS layer was annealed under vacuum at 120 °C for 12 h. The width of the interface between the PHS/PFOS and the h-PMMA layer is (55 ± 5) Å. There are several notable characteristics of the reflectivity data. At low q values, the neutron beam is almost completely reflected by the sample surface and the reflectivity is one. At q values greater than a critical angle, the reflectivity rapidly decreases. The oscillations in the reflectivity data arise from constructive and destructive

interference from neutrons reflected from interfaces in the sample. Model fits to the reflectivity data are used to determine parameters such as the film thickness, density, and interfacial width.

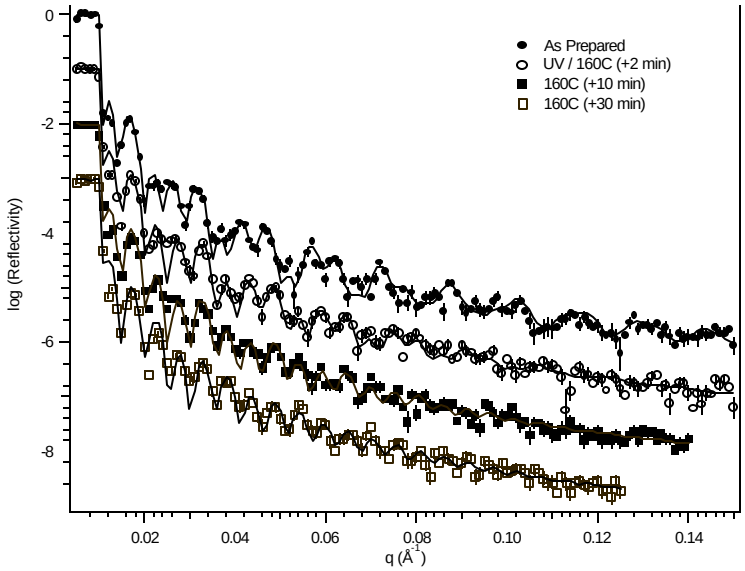

Figure 3a. The symbols are the neutron reflectivity data for a bilayer sample with a lower layer of PHS/PFOS and an upper layer of h-PMMA after various thermal treatments. The data are vertically offset for clarity and are presented with error bars representing the standard uncertainty of the measurement. The solid lines represent the best fit to the experimental data.

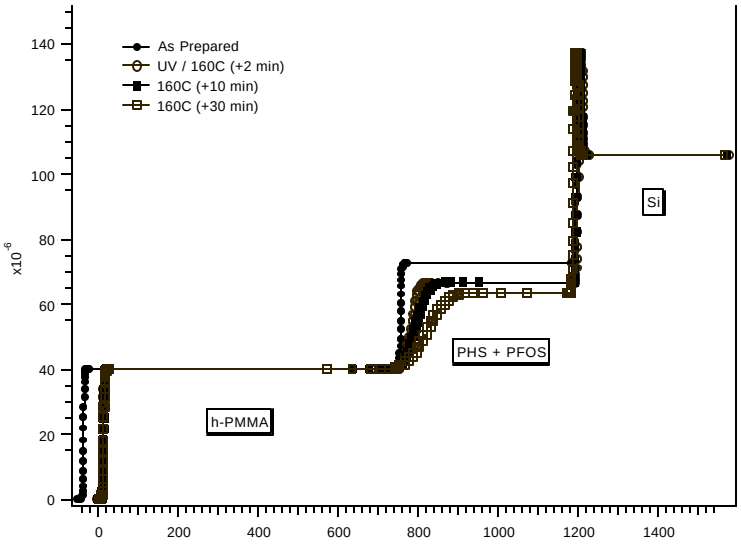

Figure 3b. Real space depth profiles representing the best model fits to the neutron reflectivity data in Figure 3a of a bilayer sample with a lower layer of PHS/PFOS and an upper layer of h-PMMA after various processing steps.

Figure 1b shows the real space profiles corresponding to the best fits to the data. Three different layers are clearly present including the h-PMMA layer, the PHS/PFOS layer, and the native oxide layer. The real space profiles are presented in terms of the neutron scattering length density determined by the elemental composition of the material and is linearly proportional to the mass density. For this sample, annealed for an extensive period, the mass density of the PHS/PFOS layer is consistent with the reported mass densities of PHS [5]. Upon exposure to UV and heating up to 4 min at 80 °C, there is no observable broadening of the interface between PHS/PFOS and h-PMMA. This is not surprising because the annealing

temperature is well below the glass transition temperatures of both PHS and PMMA. The PFOS acid has some contrast to neutrons due to the fluorine content, but the concentration levels are low enough that only significant interfacial segregation of the acid would be observed in these experiments. We do not observe any significant interfacial segregation of the acid in any of the samples discussed here.

In actual processing steps, the post-apply bake is typically no more than (1-2) min at elevated temperatures. To better compare with these processing conditions, we prepared a bilayer sample with a lower layer of PHS/PFOS (438 ± 1) Å thick and an upper layer of h-PMMA (814 ± 1) Å thick. The post-apply baking temperature was 140 °C for 3 min. The reflectivity data along with the best fits to the data are shown in Figure 2a. The real space profiles corresponding to the fits are shown in Figure 2b. We first note that the neutron scattering length density of the lower PHS/PFOS film is lower than that of the sample in Figure 1a. The shorter post-apply bake time is perhaps insufficient to remove all of the PGMEA solvent in the film or insufficient time is allowed to fully relax the film. However, after exposure to UV radiation and annealing the sample at 140 °C for varying times, there is no observable difference in the interfacial width between the PHS/PFOS and h-PMMA layers. The interfacial width after each processing step is (5 ± 1) Å. This annealing temperature is less that the Tg of PHS, but is significantly higher than the Tg of PMMA. In this sample, it appears that the glassy behavior of the PHS precludes any interfacial broadening or any evidence of significant PAG segregation to the interface.

In the next sample, we investigate the evolution of the PHS/PFOS and h-PMMA interface at a temperature above the Tg's of both polymers. Similar to the sample in Figure 2, we prepare a bilayer sample with a lower layer of PHS/PFOS (439 ± 1) Å thick and an upper layer of h-PMMA (794 ± 1) Å thick with an initial interfacial width of (5 ± 1) Å. The post-apply bake temperature for the PHS/PFOS layer was also 140 °C for 3 min. Figures 3a and 3b show the reflectivity data after various thermal treatments at 160 °C with the best fits to the data and the real space profiles corresponding to these fits, respectively. The neutron scattering length density of the PHS/PFOS layer is the same as the sample in Figure 2 prepared under identical conditions and is lower than the density of the PHS/PFOS layer after an extended post-apply bake. The post-exposure baking temperature of 160 °C is above the Tg's of both PHS and PMMA. From Figure 3b, it is clear that significant interdiffusion occurs. The location of the interface between the two layers does not remain static and moves toward the silicon substrate or into the PHS/PFOS layer. This behavior is expected because the mobilities of the two polymers are not expected to be identical [15]. The data also show that the PHS polymer apparently swells the PMMA layer with a corresponding increase in the interfacial width. For the data in Figures 3a and 3b, differences in the scattering length densities of PHS and h-PMMA are sufficiently small that these results are more qualitative than quantitative. Greater contrast and more detail in the interfacial profile can be obtained by substituting d-PMMA for h-PMMA and will be presented below. Also, these data do not provide any clear information about the effect of the acid in the polymer on the interdiffusion rates because of the relatively low concentration (and contrast) of the acid in the film.

To address the polymeric aspects of the observed transport phenomena, we performed neutron reflectivity measurements on a bilayer sample consisting of a lower layer of pure PHS (1300 ± 1) Å thick and an upper layer of d-PMMA (556 ± 1) Å thick. Deuteration of the PMMA polymer significantly enhances the contrast between the PHS and PMMA for more quantitative measurements of the polymer layer interfacial profile. The reflectivity data after different annealing times at 160 °C are shown in Figures 4a along with the best fits to the data. Figure 4b shows the real space profiles corresponding to the best fits to the data. In Figure 4a, the neutron reflectivity data show some interesting features. The as prepared bilayer sample has an interfacial width between the PHS and d-PMMA of (13 ± 1) Å and has very well defined interference oscillations. As the annealing time is increased to a total of 7 min, the interface is clearly broader, (65 ± 5) Å, because of the dampened oscillations in the reflectivity data. Interestingly, the interfacial width decreases with increased annealing time. After a total of 107 min at 160 °C, there are many more oscillations in the reflectivity data corresponding to an interfacial width of (15 ± 2) Å. Not only does the interfacial width between PHS and d-PMMA increase and then decrease, but also the position of the interface moves toward the silicon substrate and into the PHS layer. This is consistent with the data from the Figure 3a and 3b, but the increased contrast with d-PMMA provides more specific information about the interfacial profile. The real space profiles of the best fits to the reflectivity data in Figure 4b show that the PHS layer apparently swells the d-PMMA layer because of the observed decrease in the scattering length density near the interface. The d-PMMA polymer does not appear to significantly penetrate the PHS layer because the scattering length density of the PHS does not significantly change. These results again suggest that PHS and PMMA are at least partially compatible. Also, the PHS polymer is monodisperse so the swelling of the PMMA layer does not arise from the mobility of any low molecular weight fractions of the polymer distribution. The movement of the position of the interface is not unusual and has been observed in several studies of miscible polymer layers [15]. However, to the best of our knowledge, the polymeric interfacial broadening and sharpening with annealing time has not previously been reported on these length scales. These observations of

interdiffusion between PHS and PMMA are determined over length scales less than 100 Å and are relevant to interfacial broadening at the interface between areas of protected and deprotected polymers. There are still many important factors to be addressed in the future to understand the interdiffusion of PHS and PMMA. The interdiffusion rate certainly depends upon the interaction energy between the two polymers, the polymer relative molecular mass, and the relative chain mobilities as a function of the difference between the annealing temperature and the glass transition temperature of each component.

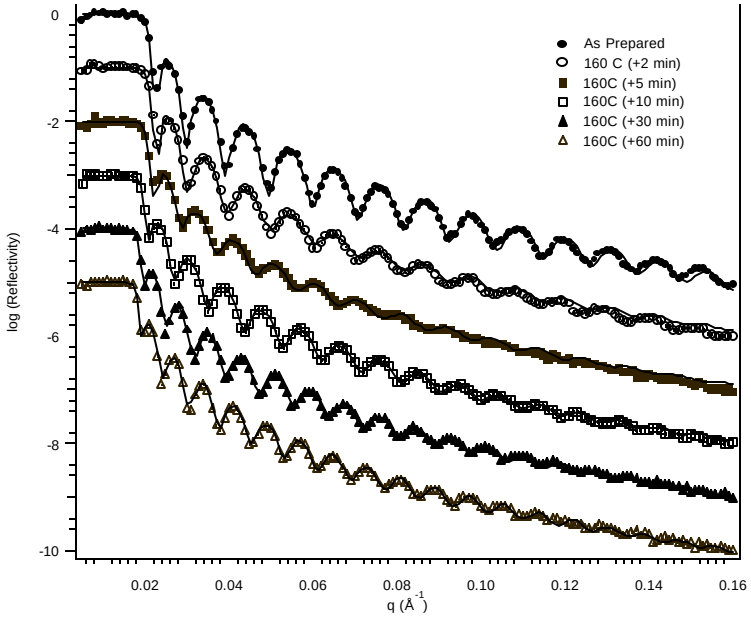

Figure 4a. The symbols are the neutron reflectivity data for a bilayer sample with a lower layer of PHS and an upper layer of d-PMMA after various thermal treatments. The data are vertically offset for clarity and are presented with error bars representing the standard uncertainty of the measurement. The solid lines represent the best fit to the experimental data.

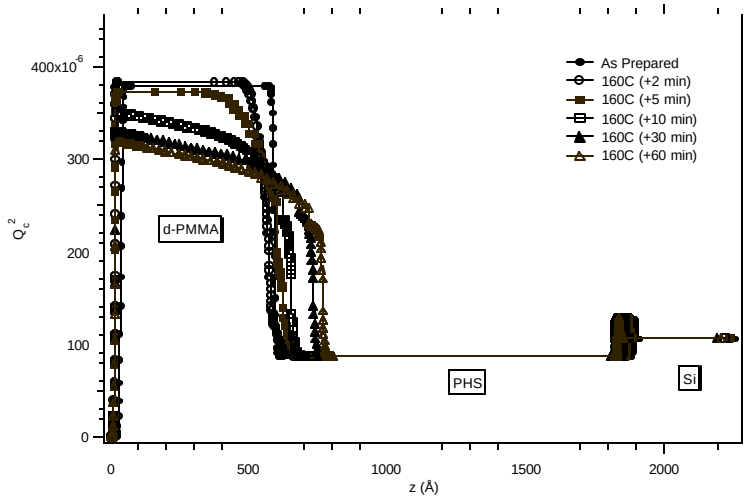

Figure 4b. Real space depth profiles representing the best model fits to the neutron reflectivity data in Figure 4a of a bilayer sample with a lower layer of PHS and an upper layer of d-PMMA after various processing steps.

In summary, we have taken advantage of the high spatial resolution of neutron reflectometry to observe the development of the interface between model photoresist polymer layers. Bilayer samples were prepared with lower layers of PHS with or without PFOS and an upper layer of either h-PMMA or d-PMMA. The samples were annealed at several temperatures above and below the glass transition temperatures for each polymer for varying times. There was not sufficient contrast to directly observe photogenerated acid diffusion after exposure because of the relatively low concentration and contrast of the acid species. No significant interfacial segregation of the acid was observed. We found that the mass density of PHS/PFOS layers that were annealed for a short time (3 min at 140 °C) was lower than for PHS/PFOS layers that were annealed for long times (12 h at 120 °C). No interdiffusion or interfacial broadening was observed for annealing temperatures lower than the glass transition temperature of PHS even if the temperature was higher than the Tg of PMMA. At temperatures above the Tg of PHS, significant interdiffusion of the PHS into the PMMA layer was observed. Interestingly, the interfacial width first increased with annealing time then decreased at longer times and the position of the interface moved toward the silicon substrate or into the PHS layer. These observations show that PHS and PMMA are at least partially miscible and suggest that interdiffusion may play a role in feature resolution when the protected and deprotected polymers are formed at the boundary between exposed and unexposed regions in a resist. In the future, we plan to enhance our understanding of the role of interfacial structure in the resolution of the lithographic process by formulating experiments to enhance the contrast of the photogenerated acid, to track the reaction front over length scales less than 20 nm, and by measuring the interaction energy between model protected and deprotected polymer photoresists.

ACKNOWLEDGEMENTS

The authors gratefully acknowledge DARPA for financial support under contract N66001-00-C-8803. The authors also benefited from helpful discussions with Dario Goldfarb and David Medeiros.

REFERENCES

1. Fedynyshyn, T. H., Thackeray, J. W., Georger, J. H., and M. D. Denison, *J. Vac. Sci. Technol. B* **12,** 3888 (1994).
2. Detinger, P. M., Lu, B., Taylor, J. W., Bukofsky, S. J., Feke, G. D., Hessman, D., and Grober, R. D., *J. Vac. Sci. Technol. B*, **16,** 3767 (1998).
3. Stewart, M. D., Postnikov, S. V., Tran, H. V., Medeiros, D. R., Nierode, M. A., Cao, T., Byers, J., Webber, S. E., and C. G. Wilson, *Proc. ACS: PMSE*, **81,** 58 (1991).
4. Barclay, G., Sundarajan, N., Xu, G., Mao, Z., Paddock, C., and C. Ober, *Proc. ACS: PMSE*, **81**, 56 (1999).
5. Lin, Q. H., private communication.
6. Postnikov, S. V., Stewart, M. D., Tran, H. V., Nierode, M. A., Medeiros, D. R., Cao, T., Byers, J., Webber, S. E., and C. G. Willson, *J. Vac. Sci. Technol. B*, **17**, 3335 (1999).
7. Lin, Q. H., Sooriyakyumaran, R., and W. S. Huang, *SPIE Proceedings* (2000) in press.
8. Lin, E. K., Kolb, R., Satija, S. K., and W. L. Wu, *Macromolecules* **32**, 3753 (1999).
9. Lin, E. K., Wu, W. L., and S. K. Satija, *Macromolecules* **30**, 7224 (1997).
10. Welp. K. A., Wool, R. P., Satija, S. K., Pipsas, S., and J. Mays, *Macromolecules*, **31**, 4915 (1998).
11. Karim, A., Felcher, G. P., and T. P. Russell, *Macromolecules*, **27**, 6973 (1994).
12. Sferrazza, M., Xiao, C., Jones, R. A. L., Bucknall, D. G., Webster, J., and J. Penfold, *Phys. Rev. Lett.*, **78**, 3693 (1997).
13. According to ISO 31-8, the term "molecular weight" has been replaced by "relative molecular mass," symbol M_r. Thus, if this nomenclature and notation were to be followed in this publication, one would write $M_{r,n}$ instead of the historically conventional M_n for the number average molecular weight, with similar changes for M_w, M_z, and M_v, and it would be called the "number average relative molecular mass." The conventional notation, rather than the ISO notation has been employed for this publication.
14. Ankner, J. F. and C. J. Makjrzak, in *Neutron Optical Devices and Applications*; SPIE Proceedings 1738; SPIE: Bellingham, WA 1992, 260.
15. Reiter, G., Huttenbach, S., Foster, M., and M. Stamm, *Macromolecules*, **24**, 1179 (1991).